AUT Journal of Electrical Engineering

AUT J. Electr. Eng., 55(1) (2023) 61-80
DOI: 10.22060/eej.2022.21587.5484

Performance Investigation of Hybrid Darrieus-Savonius Wind Turbine Compared to Straight-Bladed Darrieus Turbine by Three-Dimensional Numerical Simulation

Negar Amoozadeh*, Vahid Abbasi

Department of Electrical Engineering, Faculty of Energy, Kermanshah University of Technology, Kermanshah, Iran

ABSTRACT: Input-Parallel Output-Parallel DC-DC converters are convenient for high voltage and high current applications. One important goal of this type connection is to power-share and reduce circulating current between the converters. Therefore, control methods for power-sharing between converters should be used when the parameters mismatch. In this paper, a configuration comprising two DC-DC common grounded Z-source converters with Input-Parallel Output-Parallel connections is presented, which common grounded Z-source converter have advantages over similar converters. This study proposes two control strategies: (1) a decentralized inverse-droop control, (2) a general control strategy. Inverse-droop control is a simple method and does not need any communication between parallel converters. In the general control strategy, each converter is self-contained, and no external controller is required for achieving input/ Output Current Sharing, and a few wires are needed to create the entire system. The simulation results of an Input-Parallel Output-Parallel system comprising two common grounded Z-source converters are evaluated for investigating effectiveness of general control and inverse-droop control. It reported performance of the general control method to be better than the decentralized inverse-droop control method, which enhances the stability and dynamic characteristics of the system. The validity of the two control strategies has been studied through MATLAB simulation and the results were satisfactory.

Review History:

Received: Jul. 12, 2022
Revised: Sep. 07, 2022
Accepted: Sep. 22, 2022
Available Online: Mar. 01, 2023

Keywords:

Circulating Current
Inverse-Droop Control
Output Current Sharing
Parallel Converters
Power-Sharing

1- Introduction

The concept of microgrids (MGs) for energy production and better usage of small-scale Distributed Energy Resources (DERs) has been introduced. When Distributed Energy Resources, such as diesel generators, wind turbines, fuel cells, and photovoltaic systems, are connected to the grid, energy management becomes important. The microgrid can be used in the state of grid-connected or islanded form. It is very important to control an MG due to its automation in both islanded and grid connected modes of operation. The most important challenges in MGs protection and control include uncertainties, dynamic modeling and stability, where control and reliability issues are more significant in island mode [1]. There are many control strategies for connecting microgrids in power grids [2]. The reduction of fossil fuels and growth in energy demand have led to an interest in using renewable energy resources. Environmental issues arise due to conventional power generation [3]. These clean sources have mostly been reversed at zero minimal cost, since their progressive affect leads to less market prices [4]. DC-DC converters have many applications in renewable energy and microgrids. Therefore, a lot of research is being conducted on DC-DC converters. The combination of DC-DC converters has advantages, such as high reliability, standard modular production, and flexibility [5]. Input-Parallel Output-Parallel (IPOP) configuration allows low-power converters to be used in high-power applications. Connecting the converters in parallel is an effective and reliable method to increase the power of converters. This type of connection has several advantages: the distribution of power losses, heat stress from each power switch, and magnetic components in each converter. Parallel converters have more advantages than single converters, such as high power, centralized power supply, wise performance, higher efficiency, good dynamic response, and excellent load regulation [6]. Different reasons may make the production of circulating currents that will be explained in this paper. Circulating currents generated due to uneven values of Z-source DC-DC converter output currents will be considered in this study. Circulating current can lead to power losses. It can likewise overload converters and generate differences in current sharing [7]. One of the major objectives of the IPOP converter is the current sharing between the converters and reduction of circulating current, despite the mismatch parameters, and different control methods are used to solve this problem. Different control strategies are discussed in this research to solve the issues

*Corresponding author's email: negar.amoozadeh72@gmail.com

of equal current sharing, voltage stability, and reduction of circulating current. Many centralized and decentralized control methods have been proposed. For example, Droop-Index (DI) strategy for calculating R_{droop} in IPOP connection converters has been discussed to improve current sharing and reducing the circulating current between the converters in [2,8]. Droop control is proposed in [9]. In droop control, each converter is self-contained, controlled alone, and does not communicate with other converters; therefore, the system is reliable and flexible. In addition to the above discussed advantages, droop control has its limitations [10]. One the weaknesses of conventional droop control is that the output current is linearly increased with a decreasing output voltage, which will cause poor voltage regulation. The mismatch in output voltages can produce rise to circulating currents. Higher droop rates can produce fewer current sharing errors, but negatively influence the output voltage. Hence, there is an obvious tradeoff between current sharing and voltage regulation. A decentralized inverse-droop control method for power-sharing between Input-Series Output-Parallel (ISOP) converters is proposed in [5]. Conventional droop control method has disadvantages, such as poor voltage regulation, which the inverse-droop control method has eliminated this shortcoming. In [6], A common-duty-ratio control strategy for IPOP converters is suggested. In this method, it has the proper current sharing without direct control of the input/ Output Current Sharing. A general control for ISOP converters is proposed. The designed control can be easily implemented to all four connection architectures ISOP, IPOP, Input-Parallel Output-Series (IPOS), Input-Series Output Series (ISOS), and the converters can be connected to any number. In this scheme, not only in a steady state but also in a transient state, input/output, voltage/current can be divided [11, 12, 13]. An interleaving control strategy in [14] is proposed to improve the performance of IPOP connection converters. In this method, the interleaving control strategy will improve performance of the converters, reduce the size and stress of the input capacitor, and increase the reliability of the system. A new wireless control strategy [15] for the ISOP connection converter based on the positive output-voltage gradient technique is offered. There is no control interconnection between the converters, which increases the system's reliability. GA-based PID controller [16] is proposed for current sharing in the transient and steady-state of IPOP converters. The decentralized control [17] for ISOS connection is suggested. The main feature of this method is that it does not need a control connection link among the converters, which leads to high reliability.

Unfortunately, the conventional controller does not come up with the expected improvements to regulate the load voltage and decreasing circulating current among parallel DC-DC converters. Therefore, general control and inverse-droop techniques, are proposed to achieve this goal. The advantage of a general control strategy is that it can be used for all four connection architectures (ISOS, ISOP, IPOP, IPOS). The converter can be connected to any number. With inverse-droop control, Output Current Sharing (OCS) and Input Current Sharing (ICS) can be obtained as well. The rest of this paper is organized as follows: Section 2 presents the small-signal modeling of the common grounded Z-source converter. Next, by using the bode plots, a suitable compensator is designed. In Section 3, the operating principles of IPOP converters consisting of two DC-DC converters are described. The implementation of the inverse-droop control scheme and the general control strategy for the IPOP connection architecture are described in Sections 4 and 5. In section 6, using the bode plot, the IPOP system's stability is analyzed, and the compensator parameters are designed. The simulation results of an IPOP system consisting of two common grounded Z-source DC-DC converters are presented in Section 7. The conclusion is presented in Section 8.

2- 2. Modelling Common Grounded Z-Source DC-DC Converter

2- 1- 2.1. Configuration of the Z-Source Converter

Fig. 1 illustrates the common ground Z-source DC-DC converter. This dc-dc converter is based on the Z-source network, which consists of a conventional common Z-source network and an added diode and capacitor. The converter increases the circuit application compared to the conventional Z-source converter. It has a more efficient performance in protection issues. Additionally, the smaller inductor is another advantage of this converter [18].

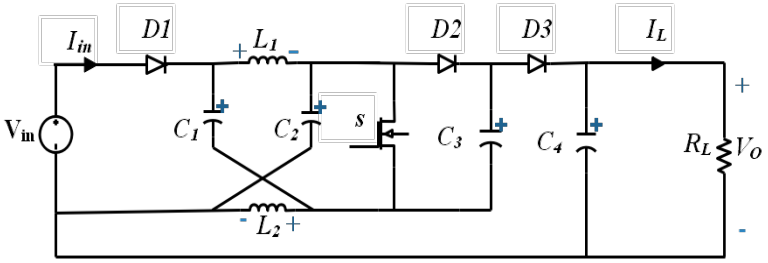

Fig. 1. Common grounded Z-source converter structure

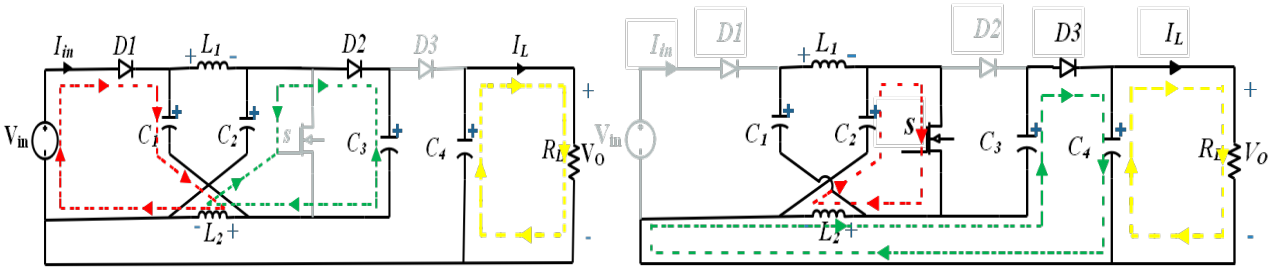

(b) (a)

Fig. 2. Switch on and off states for the common grounded Z-source converter (a) First state, the switch is on, (b) Second state, the switch is off

The converter is a DC-DC converter with two states in one switching period. These two states are called on and off. In on-state, the Switch (S) is turned on; otherwise, in off-state, the switch (S) is turned off. The analysis is performed under the theory that the inductors' current is in the same direction, and the voltage of the capacitors is constant. To complete the DC-DC converter analysis, its dynamic state has been investigated, which is used to design a suitable compensator. Study of transient and stability performance require the small-signal model of the converter [19]. In state-space modeling, state-space equations are obtained for each converter state [20]. Analysis of the State-Space Average model (SSA) of the DC-DC converter is calculated by considering two assumptions1 :) The converter operates in CCM mode 2) All converter components are ideal. First, the equations of the State-Space Average model are obtained for the converter shown in Fig.1. Next, using the equations, transfer functions for the converter are obtained. Using the transfer functions and the bode diagram, the controller is designed.

2- 2- Analysis of On-State

Due to the impedance network's symmetrical structure, the inductor currents L_1 and L_2 are equal during operation. Additionally, in steady-state and transient conditions, the voltage of capacitors C_1 and C_2 is equal. During on-state, the switch is on and there are three loops, as mentioned in Fig. 2*a*. In on-state, diodes D_1 and D_2 are blocking, and diode D_3 is conducting. The first loop consists of L_2 - C_1, and the second loop consists of L_2, C_3, C_4, D_3. The third loop is the load (R) and the capacitor C_4. Using the equivalent circuits of the switching states in Fig. 2*a*, the state-space model of on-state can be written as:

$$\dot{X} = A_{ON}X + B_{ON}U \Rightarrow \begin{bmatrix} \frac{di_L}{dt} \\ \frac{dV_C}{dt} \\ \frac{dV_{C3}}{dt} \\ \frac{dV_{C4}}{dt} \end{bmatrix} = \begin{bmatrix} 0 & \frac{1}{L} & 0 & 0 \\ -\frac{1}{C} & 0 & 0 & 0 \\ \frac{1}{2C} & 0 & 0 & \frac{-1}{2CR} \\ \frac{-1}{2C} & 0 & 0 & -\frac{1}{2CR} \end{bmatrix} X + \begin{bmatrix} 0 & 0 \\ 0 & 0 \\ 0 & 0 \\ 0 & 0 \end{bmatrix} \times \begin{bmatrix} V_{in} \\ i_{in} \end{bmatrix} \quad (1)$$

2- 3- Analysis of Off-State

During the off state operation, the switch is off and the circuit contains three loops, as shown in Fig. 2*b*. When the switch is off, diode D_3 is blocking and diodes D_1 and D_2 are on. The first loop consists of the voltage source and diode D_1, capacitor C_1, and inductor L_2, and the second loop consists of inductor L_2, capacitor C_2, diode D_2, and capacitor C_3. Capacitor C_4 is discharged in the last loop, causing the load current to be continuous and not interrupted. Using the equivalent circuits of off-state in Fig. 2*b*, state-space models of off-state can be written as:

$$\dot{X} = A_{OFF}X + B_{OFF}U \Rightarrow \begin{bmatrix} \frac{di_L}{dt} \\ \frac{dV_C}{dt} \\ \frac{dV_{C3}}{dt} \\ \frac{dV_{C4}}{dt} \end{bmatrix} = \begin{bmatrix} 0 & -\frac{1}{L} & 0 & 0 \\ -\frac{1}{C} & 0 & 0 & 0 \\ \frac{2}{C} & 0 & 0 & 0 \\ 0 & 0 & 0 & -\frac{1}{C \times R} \end{bmatrix} X + \begin{bmatrix} \frac{1}{L} & 0 \\ 0 & \frac{1}{C} \\ 0 & -\frac{1}{C} \\ 0 & 0 \end{bmatrix} \begin{bmatrix} V_{in} \\ i_{in} \end{bmatrix} \quad (2)$$

Therefore, *x*.vector of the converter is defined as follows:

$$X(t) = \begin{bmatrix} i_L & V_C & V_{C3} & V_{C4} \end{bmatrix}^T \quad (3)$$

The input vector(*u*) is defined as follows:

$$u(t) = \begin{bmatrix} v_{in} & i_{in} \end{bmatrix}^T \quad (4)$$

Small-signal analysis is used to get transfer functions of the converter. Small signal models are obtainable with perturbation theory in the State-Space Averaged models [21]. According to the small-signal method [21], input voltage, state variables and duty cycle (d), and output voltage consist of two parts: DC values (*U, V_O, X, D*) and perturbations ($\hat{u}, \hat{v}_o, \hat{x}, \hat{d}$) that are:

$$u = U + \hat{u}, v_o = V_O + \hat{v}_o, x = X + \hat{x}, d = D + \hat{d} \quad (5)$$

Small-signal model is as follows:

$$\frac{d\hat{x}}{dt} = A_{avg}\hat{x} + B_{avg}\hat{u} + \left[\left(A_{on} - A_{off}\right)X + \left(B_{on} - B_{off}\right)U\right] \times \hat{d} \quad (6)$$

A_{avg} and B_{avg} are calculated as follows:

$$\begin{aligned} A_{avg} &= D \times A_{on} + (1-D) \times A_{off} \\ B_{avg} &= D \times B_{on} + (1-D) \times B_{off} \end{aligned} \quad (7)$$

According to (1), (2), (6), and (7) the small-signal models are as follows:

$$\begin{cases} LS\hat{i}_L(s) = (2D-1)\hat{v}_c(s) + (1-D) \\ \hat{v}_{in}(s) + 2\hat{d}V_C(s) - \hat{d}V_{in}(s) \\ CS\hat{v}_c(s) = -\hat{i}_L(s) + (1-D)\hat{i}_{in}(s) - \hat{d}I_{in}(s) \\ CS\hat{v}_{c3}(s) = (\frac{4-3D}{2})\hat{i}_L(s) + (D-1)\hat{i}_{in}(s) + \\ (\frac{-D}{2R})\hat{v}_{c4}(s) - \frac{3}{2}\hat{d}I_L(s) + \hat{d}I_{in}(s) + (\frac{1}{2R} \times V_{C4}(s) \times \hat{d}) \\ CS\hat{v}_{c4}(s) = (\frac{-2+D}{2R})\hat{v}_{c4}(s) + (\frac{-D}{2})\hat{i}_L(s) - \\ (\frac{1}{2} \times I_L(s) \times \hat{d}) + (\frac{1}{2R} \times V_{C4}(s) \times \hat{d}) \end{cases} \quad (8)$$

With respect to the small-signal models of the converter, open-loop transfer functions can be obtained as follows:

$$\begin{aligned} G_{Vd}(s) = \frac{\hat{v}_o}{\hat{d}} = & \frac{((2D-1) \times -DR \times I_{in})}{(2RCS + 2 - D) \times (LCS^2 + 2D - 1)} + \\ & \frac{(-2RDLC \times V_C \times S^2)}{(2RCS + 2 - D) \times (LCS^2 + 2D - 1)} + \\ & \frac{\left(\left(-RI_L + V_O\right) \times (LCS^2 + 2D - 1)\right)}{(2RCS + 2 - D) \times (LCS^2 + 2D - 1)} + \\ & \frac{4R(LCS^2 + 2D - 1)}{(2RCS + 2 - D) \times (DLCS^2 \times V_{in})} \end{aligned} \quad (9)$$

Table 1. Key parameters values

parameters	symbol	values
input voltage	V_{in}	30 V
output voltage	V_O	240 V
individual	L_1, L_2	1 mH
Individual	C_1, C_2, C_3	680 μF
output capacitor	C_4	680 μF
switching frequency	f_{sw}	25 kHz
resistive load	R_L	250 Ω
duty cycle	D	0.4

$$G_{Vin}(s)=\frac{\hat{v}_o}{\hat{v}_{in}}=\frac{-D(1-D)RC\times S}{(LCS^2+2D-1)\times(2RCS+2-D)} \quad (10)$$

$$G_{Viin}(s)=\frac{\hat{v}_o}{\hat{i}_{in}}=\frac{-DLR(1-D)\times S}{(LCS^2+2D-1)\times(2RCS+2-D)} \quad (11)$$

Rated circuit parameters values are shown in Table 1.

According to the values of Table (1) in G_{vd} per d=0.4 and R=250Ω, a zero is seen on the right-half of the S-plane (RHP zero), which makes the system unstable. To solve the instability, by using the Bode diagrams, the parameters of the compensator for G_{vd}, G_{vin}, and G_{iin} are designed. Phase margins of the transfer functions with PM are shown in Fig. 3. Considering the starting phase (360°+), the criterion for measuring the phase margin is +180°. As can be seen from Fig. 3a, the phase margin of G_{vd} is +90°. To achieve the desired phase margin (40°-60°), The compensator is calculated by Eq. (12).

$$G_c=10\times\frac{(s+100)}{(s+10)} \quad (12)$$

As it can be seen from Fig. 3a, the phase margin for G_{vd} is decreased to 41.5°. The compensator of the G_{vin} is as below:

$$G_c=0.1275\times\frac{(1+0.22s)(1+190s)}{s(1+2.4e^{-6}s)(1-1.8s)} \quad (13)$$

As shown in Fig. 3b, the phase margin and gain margin for G_{vin} after compensation are 45.1° and 5 dB, respectively. The compensator of the G_{iin} is defined as follows:

$$G_c=0.1875\times\frac{(1+0.24s)(1+350s)}{s(1+6.7e^{-7}s)(1-6.3s)} \quad (14)$$

According to Fig. 3c, the phase margin and gain margin for G_{iin} after compensation are 59.1° and 6 dB, respectively.

3- Principles of Operation of IPOP Converters Consisting of Two Common Grounded DC-DC Converters

The IPOP structure consisting of two common grounded Z-source converters, is shown in Fig. 4. This type of connection allows the components of each converter to withstand part of the total power. V_{in} is the input voltage, and I_{in1}, I_{in2} and I_{in} are the input current of the first converter, second converter, and the input current, respectively. I_{o1}, I_{o2}, and I_L are the output current of the first and second converters and the load current, respectively. Assuming that all the parameters of the two converters are same and the system is in a steady state.

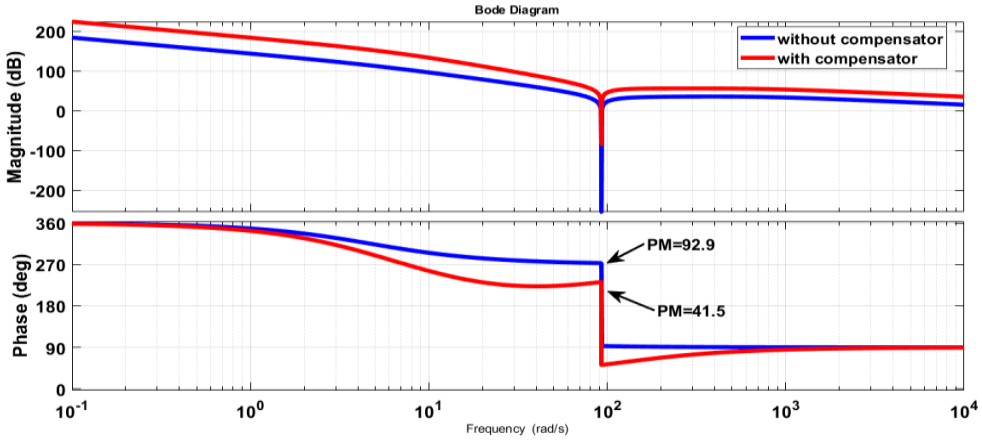

(a)

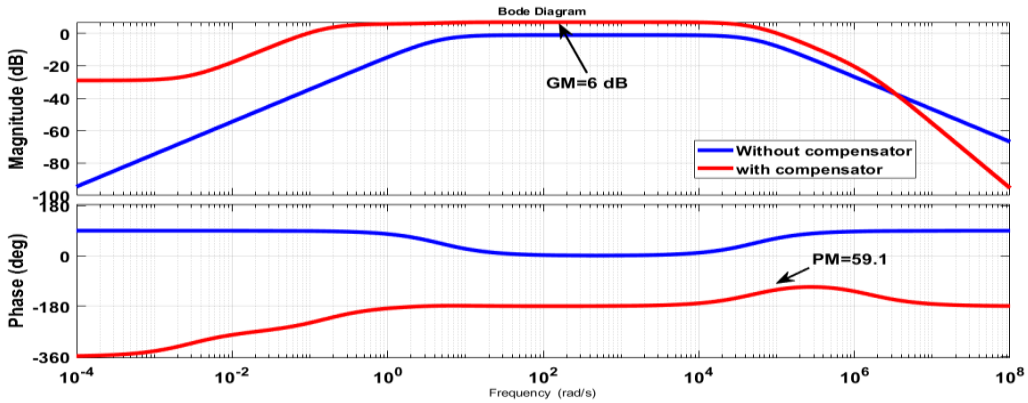

(b)

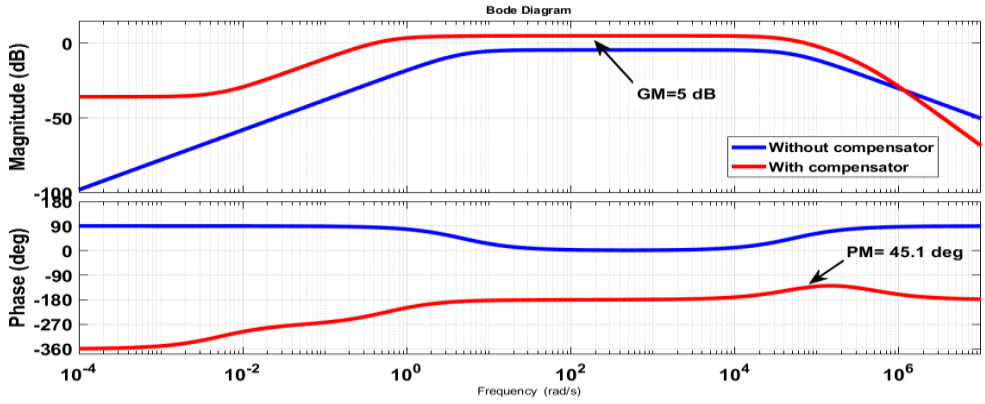

(c)

Fig. 3. Bode diagrams of the transfer functions for D= 0.4, and the parameters in Table 1 (a) $G_{vd}(s)=\hat{V}_o(s)/\hat{d}(s)$ (b) $G_{vin}(s)=\hat{V}_o(s)/\hat{V}_{in}(s)$ (c) $G_{iin}(s)=\hat{V}_o(s)/\hat{I}_{in}(s)$

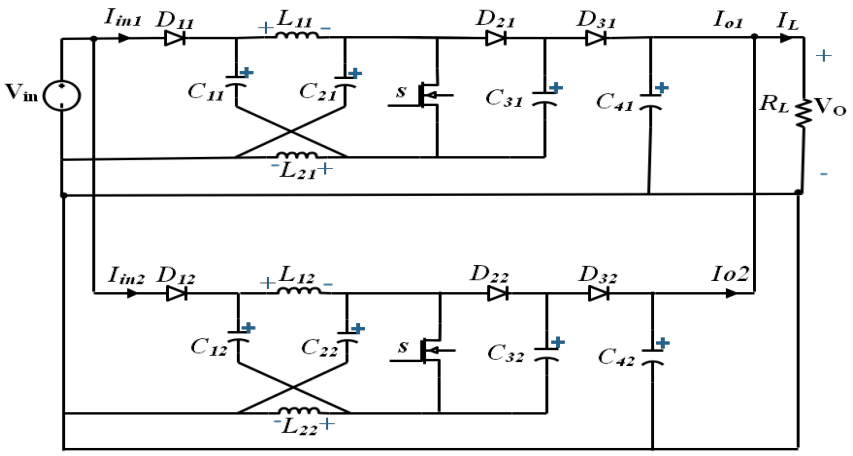

Fig. 4. The topology of the IPOP system

3- 1- IPOP DC-DC Converter Small-Signal Analysis

Using the small-signal model of the common ground Z-source converter, the small-signal model for the IPOP system consisting of two common grounded Z-source converters is calculated. By substituting I_{in}/n instead of I_{in} and I_O/n instead of I_L (n denotes the number of converters), the resistance load of each converter is nR_L. The small-signal models are as follows:

$$\begin{cases} LS\hat{i}_L(s)=(2D-1)\hat{v}_c(s)+(1-D)\\ \hat{v}_{in}(s)+2\hat{d}V_C(s)-\hat{d}V_{in}(s)\\ CS\hat{v}_c(s)=-\hat{i}_L(s)+(1-D)\hat{i}_{in}(s)-\hat{d}\,I_{in}/n\,(s)\\ CS\hat{v}_{c3}(s)=(\dfrac{4-3D}{2})\hat{i}_L(s)+(D-1)\hat{i}_{in}(s)+\\ (\dfrac{-D}{2nR})\hat{v}_{c4}(s)-\dfrac{3}{2}\hat{d}\,I_L(s)+\hat{d}\,I_{in}/n\,(s)+\\ (\dfrac{1}{2nR}\times V_{C4}(s)\times\hat{d})\\ CSV_{c4}(s)=(\dfrac{-2+D}{2nR})\hat{v}_{c4}(s)+(\dfrac{-D}{2})\hat{i}_L(s)-\\ (\dfrac{1}{2}\times I_L(s)\times\hat{d})+(\dfrac{1}{2nR}\times V_{C4}(s)\times\hat{d}) \end{cases} \quad (15)$$

The transfer functions are as follows:

$$\begin{aligned} G_{Vd}=&\frac{((2D-1)\times -DR\times I_{in})}{(2nRCS+2-D)\times(LCS^2+2D-1)}+\\ &\frac{(-2nRDLC\times V_C\times S^2)}{(2nRCS+2-D)\times(LCS^2+2D-1)}+\\ &\frac{\left((-nRI_L+V_O)\times(LCS^2+2D-1)\right)}{(2nRCS+2-D)\times(LCS^2+2D-1)}+\\ &\frac{4nR(LCS^2+2D-1)}{(2nRCS+2-D)\times(DLCS^2\times V_g)} \end{aligned} \quad (16)$$

$$\begin{aligned} G_{id}=&\frac{\hat{i}_o}{\hat{d}}=\frac{DI_g/n(2D-1)-2DCV_CS-CV_gDS}{(LCS^2+2D-1)(2nRCS+2-D)}\\ &+\frac{1}{2}(I_O/n-I_L) \end{aligned} \quad (17)$$

The main purpose of the IPOP connection is to power-share and reduce the circulating current among the system's converters. For this purpose, sharing input current and output current equally between the converters of the IPOP system needs control methods. Parameter's mismatch of the parallel connected converters disrupts the system. For power-sharing between the converters, despite such disturbances, the system must keep up its stable state. Therefore, the following two control methods have been used in this paper:

1. Inverse-Droop Control
2. General Control Strategy

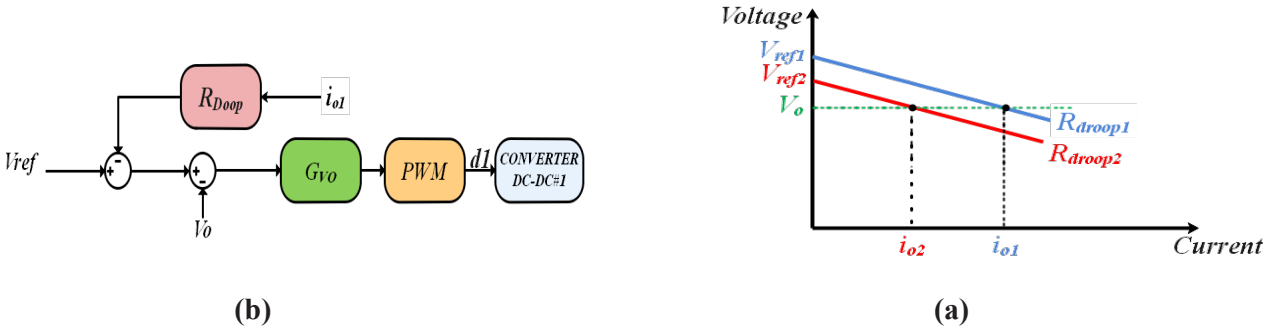

Fig. 5. Conventional droop control (a) Droop regulation characteristic of two paralleled converters with resistive load (b) Control diagram for module #1

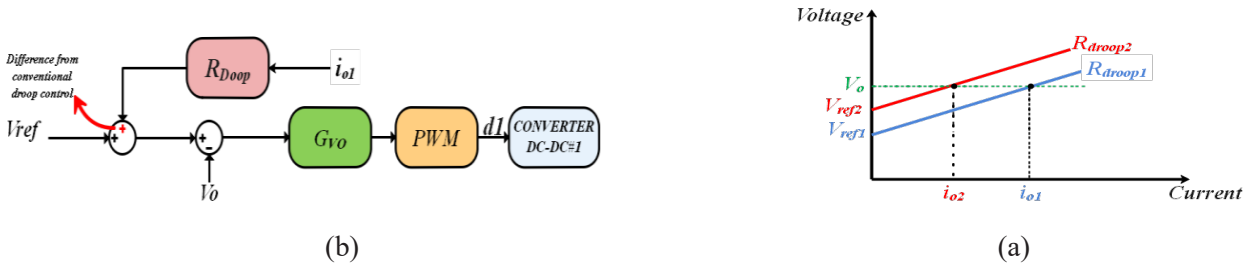

Fig. 6 Inverse-droop control (a) Inverse-droop regulation characteristic of two paralleled converters with resistive load (b) Control diagram for module #1

4- Operation Principle of IPOP Converters with Inverse-Droop Control

Conventional droop control strategy is based on the output voltage droop when the load current increases. The best power-sharing between the converters is created with the method based on adjusting the output impedance. The current sharing based on the droop control strategy depends on the slope of the load regulation curve of the parallel connection converters. The output voltage of each converter decreases as the output current increases. The relation between the output current and voltage reference indicates as follows [22]:

$$V_{ref} - V_{oj} = i_{oj}(R_{droopj}) \tag{18}$$

V_{ref}, V_{oj} (j=1, 2…, n), i_{oj}, and R_{droopj} are the reference voltage, the output voltage, the output current and the droop virtual resistance, respectively. The conventional droop regulation characteristic of two converters is shown in Fig. 5. As can be seen, current sharing can be achieved well, but the voltage regulation weakens and output power loss increases with an increase in R_{droop}. The power- sharing is improved with this control strategy [23]. Fig. 5b illustrates a conventional droop control diagram, and $V_{ref,}$ V_o, and R_{droop} are the output voltage reference, feedback of output voltage, and the droop coefficient, respectively.

Fig. 6 depicts the decentralized inverse-droop control. The difference between the conventional droop control with inverse-droop control is the positive feedback polarity of the output current instead of negative polarity.

The inverse-droop control diagram for IPOP DC-DC converters is mentioned in Fig. 7. As illustrated, there is no Input Current Feedback. Thus, the ICS loop does not exist in control. The ICS can be obtained when OCS is obtained and vice versa. Therefore, the diagram block of each converter only uses the output current and the output voltage of the converter. Consequently, it is decentralized, and no communication is needed between the controllers. For G_{VO}, a PI controller is used (G_{vo} is G_{vd}); the coefficients of this controller are calculated from the bode plot.

4- 1- Output Current Sharing and Circulating Current

Fig. 8 shows steady-state equivalent circuit of two parallel connected DC-DC converters [2], where V_{DC1}, V_{DC2}, I_{O1}, I_{O2}, R_1, R_2, and I_{C12} are output voltages of converter 1 and converter 2, the output currents, the cable resistances, and the circulating current between the two converters, respectively. To divide the output current and the circulating current based on the output voltages of the converters, resistance of the cables for all four connection architectures are listed in Table 2] 2]. Connecting a series resistor (R_{droop}) with each converter reduces the circulating current.

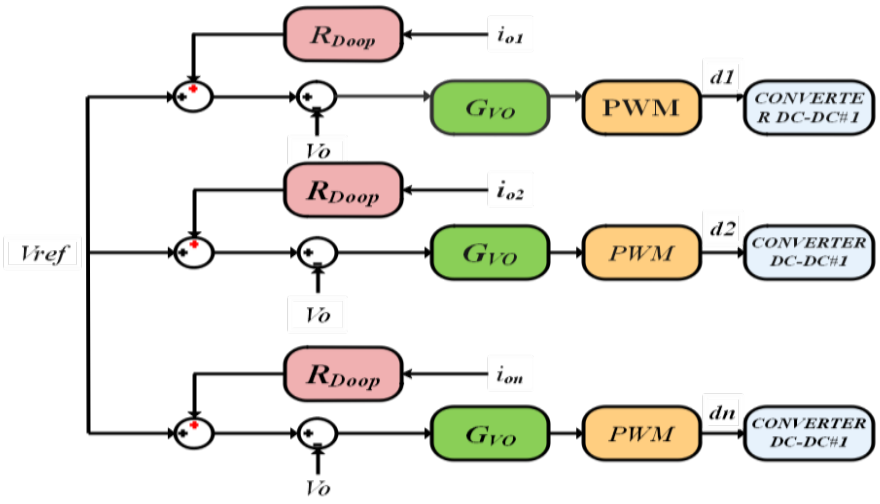

Fig. 7. Inverse-droop control diagram for n-module IPOP DC-DC converter

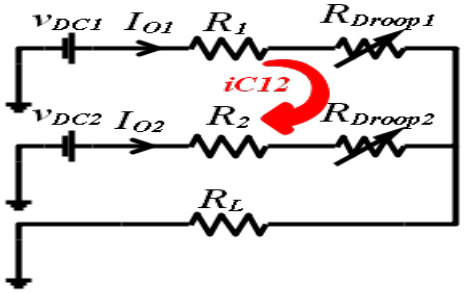

Fig. 8. equivalent circuit for the dc output side

Table 2. Case studies for load sharing and circulating current

case	I_{O1}, I_{O2}	V_{DC1}, V_{DC2}	R_1, R_2	I_{C12}/I_{C21}
1	equal	equal	equal	0
2	different	equal	different	0
3	different	different	equal	Not zero
4	different	different	different	Not zero

Based on Kirchhoff's law (KVL) in Fig. 8 [2]:

$$V_{DC1} - R_1 I_{o1} - R_L I_L = 0$$
$$V_{DC2} - R_2 I_{o2} - R_L I_L = 0 \quad (19)$$

The output currents in the converters are as follows:

$$I_{o1} = \frac{(R_2 + R_L)V_{DC1} - R_L V_{DC2}}{R_1 R_2 + R_1 R_L + R_2 R_L} \quad (20)$$

$$I_{o2} = \frac{(R_1 + R_L)V_{DC2} - R_L V_{DC1}}{R_1 R_2 + R_1 R_L + R_2 R_L} \quad (21)$$

$$I_{C12} = -I_{C21} = \frac{V_{DC1} - V_{DC2}}{R_1 + R_2} = \begin{cases} \frac{I_1 - I_2}{2}; R_1 = R_2 \\ \frac{I_1 R_1 - I_2 R_2}{R_1 + R_2}; R_1 \neq R_2 \end{cases} \quad (22)$$

According to (22) in parallel connection converters, if the output current difference between the two converters is zero, the circulating current becomes zero.

4- 2- Droop-Index Calculation

Droop-Index (DI) is a function of the normalized output currents difference and output power loss. Due to the DI, the proper droop coefficient (R_{Droop}) can be obtained [2].

$$Droopindex = \min[\frac{1}{2}\left(\left|I_{o1} - I_{o2}\right|_{Ni} + \left(P_{loss}\right)_{Np}\right)] \quad (23)$$

N_i and N_p are stands for normalization of current sharing difference based on the rated load current and output power loss based on maximum acceptable losses in terms of converter rated power, respectively.

$$x = \frac{V_{DC1}}{V_{DC2}}, y = \frac{R_1}{R_2}, m = R_2 + R_{droop2} \quad (24)$$

$$R_{droop1} = yR_{droop2} \quad (25)$$

Power losses and current differences are calculated as follows:

$$P_{loss} = I_{o1}^2(R_1 + R_{Droop1}) + I_{o2}^2(R_2 + R_{Droop2}) \quad (26)$$

$$\left|I_{o1} - I_{o2}\right| = \left|\frac{mV_{DC2} - myV_{DC2} + 2(x-1)V_{DC2}R_L}{m^2 y + mR_L(y+1)}\right| \quad (27)$$

The relationship between the normalized output current difference and normalized losses with respect to the parameters of Tables (1), (26), and (27) is demonstrated in Fig9 .

It is obviously shown that by increasing R_{droop}, the output power decrease. Thus, the efficiency decreases and the output current difference is reduced. Fig. 9 depicts the proper R_{Droop} value, which is equal to 0.29.

5- General Control Strategy

In general control, at least two control loops are required in the four connection architectures, one loop to regulate the converter's output voltage and another control loop to divide input voltages/currents or output voltages/currents. The two control loops operate by varying the duty cycles of the converters. The different duty cycle may affect both the converter output voltage and the sharing input/output voltage/current converters. Therefore, these two control loops may be coupled and lead to problems in the design of the loops. The proposed general control strategy separates the two control loops. As illustrated in Fig. 10, a general control method is suggested for DC-DC converters in four connection architectures. The output voltage control loop of the system ensures the desired output voltage of the system. $V_{o\text{-}EA}$ denotes the control signal that is the result of regulates the output voltage, which is used to generate the common signal duty cycle d_{vo_j} (j = 1, 2…, n). V_{sh_g} is the control signal average value of total input/output, voltages/currents, divided between the converters, and V_{shj} (j = 1,2…, n) indicates the input or output variable of each converter. For IPOP systems, V_{sh_g} is the I_O/n, and V_{shj} is the output current of each converter. These signals are fully described in Table. 3. It shows that the general control strategy of the Output Voltage Regulation loop of the system decouples the input/output variable sharing loops.

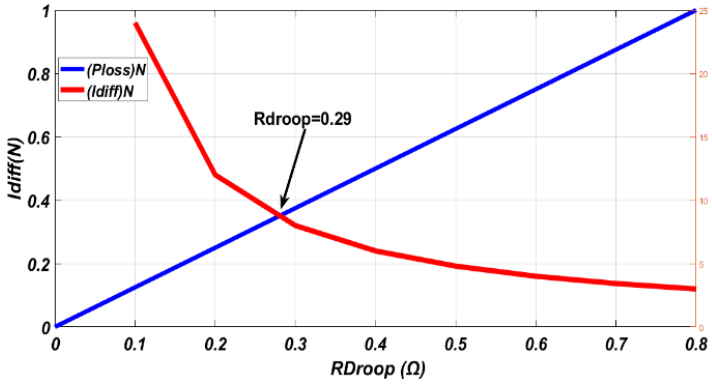

Fig. 9. Relations between normalized output current difference and output power loss with variation in Rdroop

Table 3. Introduction of general control method inputs for four connection architectures

Architecture	V_{shj} (j=1, 2…, n)	V_{sh-g}
IPOP	I_{inj} or I_{oj}	I_{in}/n or I_o/n
IPOS	I_{inj} or V_{oj}	I_{in}/n or V_o/n
ISOP	V_{inj} or I_{oj}	V_{in}/n or I_o/n
ISOS	V_{inj} or V_{oj}	V_{in}/n or V_o/n

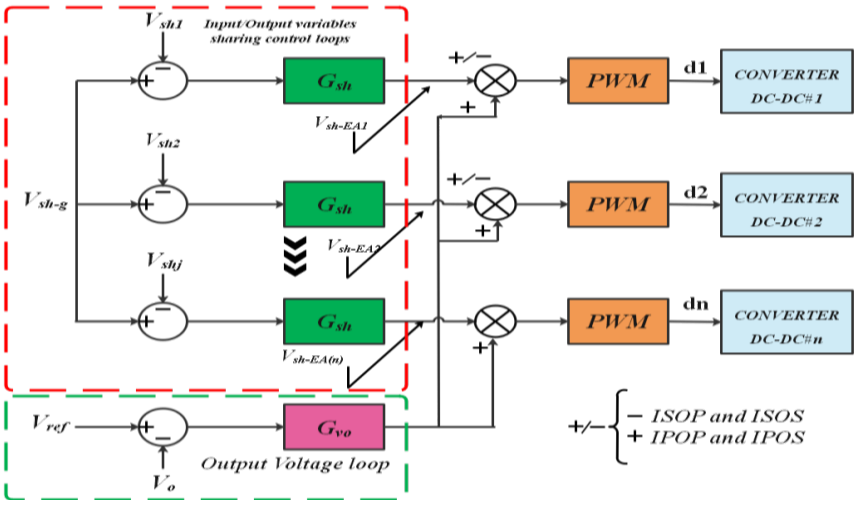

Fig. 10. General control strategy for series-parallel DC-DC converters

5- 1- OVR and OCS Loops Gain

As described in the Table. 3, for parallel connection DC-DC converters, Output Current Feedback (OCF), or Input Current Feedback (ICF) control scheme is used. In this paper, the OCF control theory is used. The OCF control scheme consists of two control loops, a common loop of Output Voltage Regulation (OVR) and individual loops of OCS. In each loop, a compensator is used to adjust the stability of the system. To use the bod plot criterion for stability of the system, loops gain is required, which OVR loop gain and OCS loop gain are:

$$T_{vo}(s) = -nK_{vd}G_{vo}(s)G_{vd}(s)/V_M \quad (28)$$

$$T_{io}(s) = K_{id}G_{io}(s)G_{id}(s)/V_M \quad (29)$$

6- Stability Analysis for Two IPOP Common Grounded Z-source DC-DC Converters

Compensator parameters of the gain loops are designed using the bode plots. Using gain and phase margin, the distance between the system and the instability boundary is determined. For the design of OCS and OVR loops gain, an IPOP system consisting of two Z-source converters according to the parameters of Table (1) is considered. Substituting (16) into (28) the bode plot for OVR loop gain, as can be noticed in Fig. 11. In the case without a compensator, the gain crossover frequency, the phase margin, and the phase crossover frequency are 15.4 Hz, -88.6° and infinite, respectively, that demonstrate instability of the system. However, small phase margin causes low damping and high overshoot.

A proper phase margin improves the system transient response. The PI compensator transfer function for the OVR loop gain is as follows:

$$G_{vo} = 0.001 + \frac{0.025}{s} \quad (30)$$

Bode plots of the OVR loop gain with the compensator and without compensator are shown in Fig. 11 (the phase margin is 66.1°after the compensation). If all interconnected converters had the same parameters, the existence of an OCS control loop was unnecessary. However, parameters mismatch is not possible in practice. Therefore, the OCS control loop is required. Substituting (17) into (29) bode plot for OCS loop gain is shown in Fig. 12. OCS loop feedback is positive, and loop gain is negative. In Figure. 12, by removing the negative link, the criterion for measuring the phase margin is +180°, which shows instability of the system. To stable the system, a PID compensator for the OCS loop gain is obtained as follows:

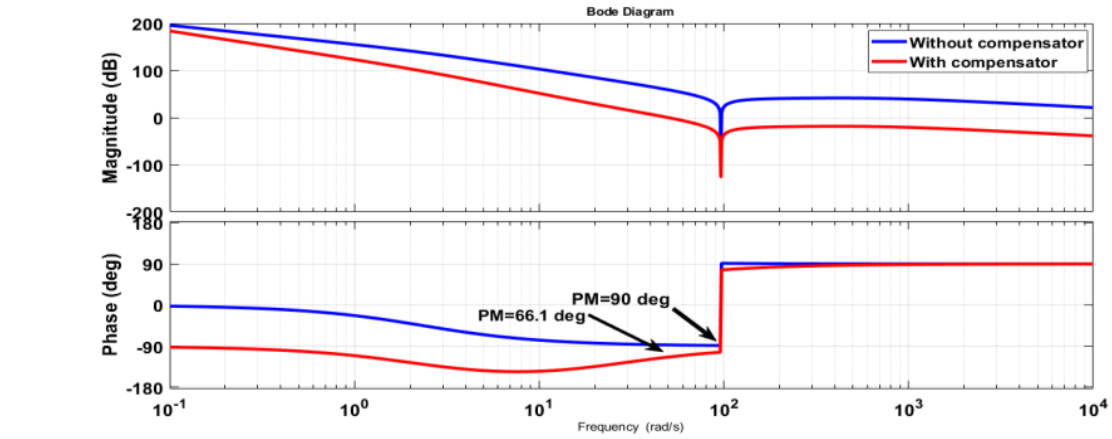

Fig. 11. Bode plot for OVR loop gain with compensator and without compensator

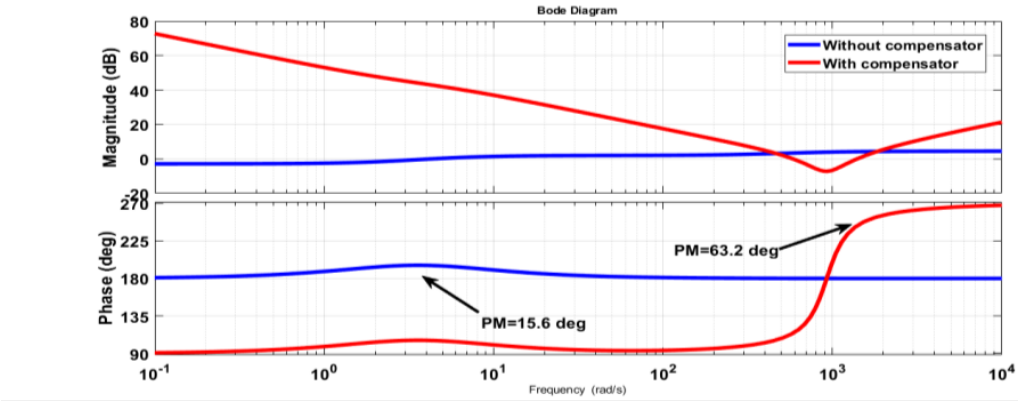

Fig. 12. Bode plot for OCS loop gain with compensator and without compensator

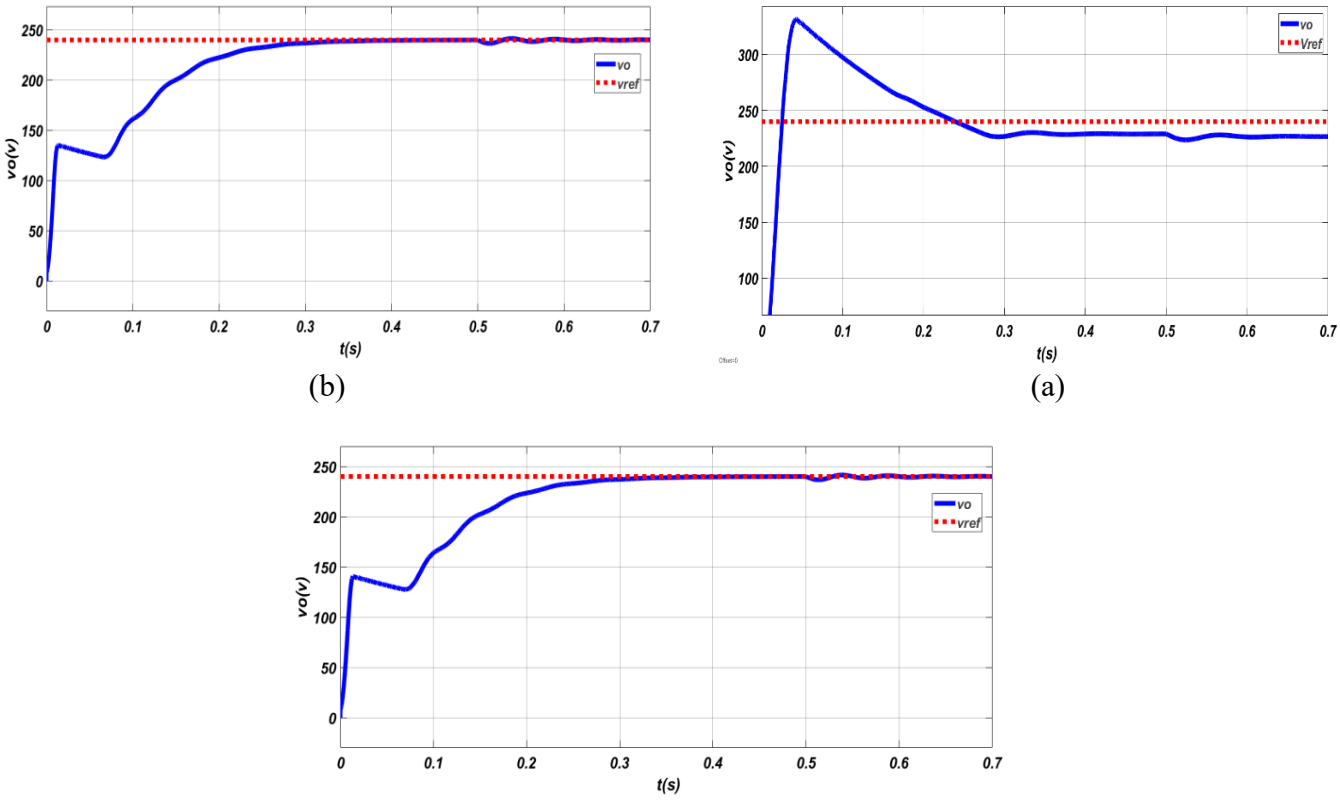

Fig. 13. Output voltages (a) without control (b) with inverse-droop control (c) with general control

Table 4. Comparison of output voltages in three methods

Time(s)	Vo (withoutcontrol)	Vo (inversedroop)	Vo (general control)
0-0.1	297.4	161.1	163.6
0.1-0.3	226.3	237	237
0.3-0.5	229	239	239
0.5-0.7	226	240	240

$$G_{io} = 0.278 + \frac{600}{s} + 0.0007s \qquad (31)$$

According to Fig. 12, the phase margin after the compensation is 63.2°.

7- Simulation Results

According to Table 1 and using the simulation results, a comparison among the without control, the inverse-droop control, and general control strategy in the mismatch of parameters is performed ($L_{11,}$ L_{21}=1mH and $L_{12,}$ L_{22}=1.5mH) and (C_{11}, C_{21}, $C_{31,}$ C_{41}=680µF and C_{12}, C_{22}, $C_{32,}$ C_{42}=680µF). The simulation shows the output voltage response, output currents and input currents, and circulating current when the input voltage is 30V, and when in time 0.5s the R_{load} from 250Ω to 125Ω in the conditions that parameters mismatch.

7- 1- Output Voltage Simulation Results

Fig13. , displays the output voltage without control, with the inverse-droop control and the general control strategy despite the parameters mismatch. By comparing these three methods, it can be perceived that in the mismatch technique x, the output voltage does not reach the reference voltage (240V) and has a voltage drop of 11V. However, in the two methods of droop and general control, the voltage has remained well constant at the reference voltage of (240V). As shown in Fig. 13 and Table 4, voltage of the system without control method stabilizes in over 0.4 seconds, but the system with the inverse-droop and general control voltage stabilizes in less than 0.4 seconds.

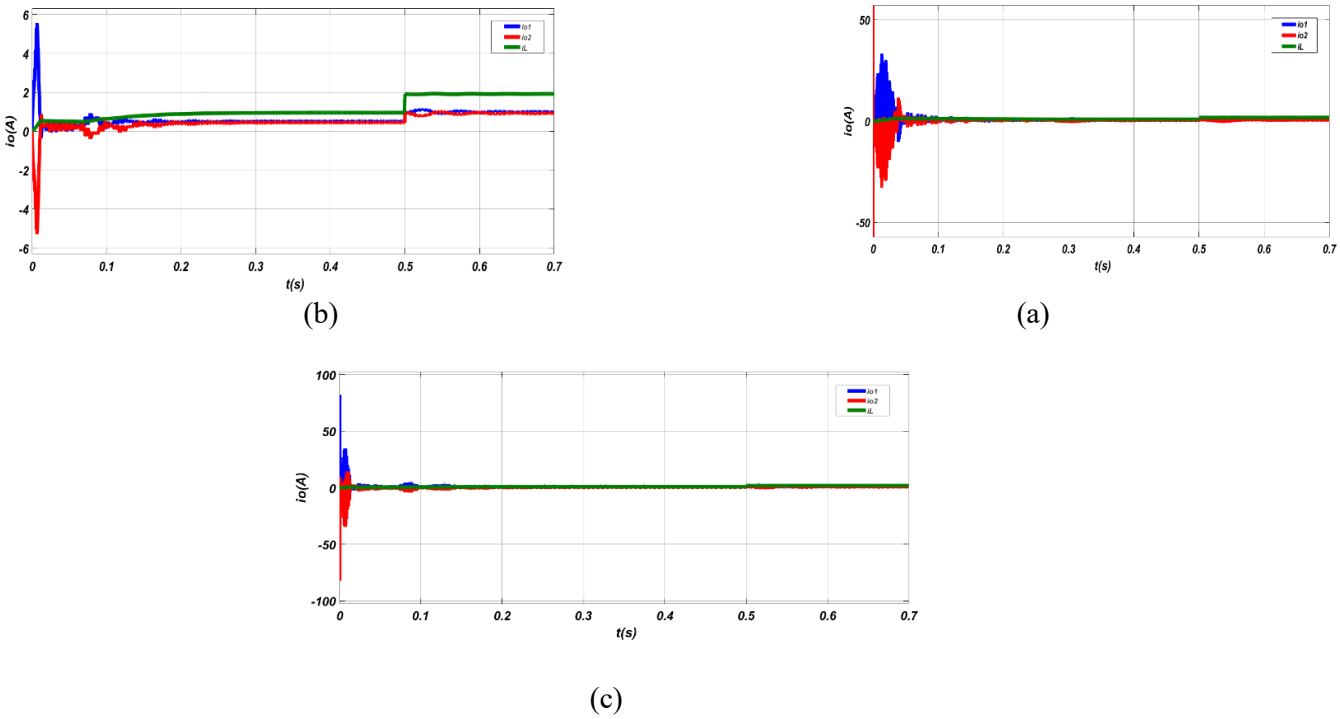

Fig. 14. Output currents (a) without control (b) with inverse-droop control (c) with general control

Table 5. Comparison of the output currents in three methods

Time(s)	I_{O1}-I_{O2}-I_L(A) (withoutcontrol)	I_{O1}-I_{O2}-I_L(A)(inversedroop)	I_{O1}-I_{O2}-I_L(A) (generalcontrol)
0-0.1	0.55-0.63-11.9	0.33-0.31-0.64	0.32-0.32-0.65
0.1-0.3	0.4-0.49-0.9	0.47-0.47-0.94	0.47-0.47-0.95
0.3-0.5	0.41-0.5-0.91	0.49-0.46-0.96	0.48-0.48-0.96
0.5-0.7	0.82-0.98-1.8	0.97-0.94-1.92	0.96-0.96-1.92

7- 2- Output Currents and Load Current of Simulation

As can be seen in Fig14., the output currents and load current without control, with the inverse-droop control and with the general control strategy are the mismatch parameters. Comparison between the methods validates current sharing between the converters when inverse-droop control and general control are used. According to the parameter values, the nominal load current is 0.96 A, so each of the converters has a nominal output current of 0.48A. Referring to Fig. 14, and Table 5, the general control method divides the currents more accurately and better than the other two techniques.

7- 3- Input Currents Simulation Results

Fig15. shows the input currents without the control method, with inverse-droop control and general control. By comparing the three methods, it seems that current sharing among two converters is better in the two methods with controllers. According to Table 1, nominal total input current is 7.68 A, so each of the converters has a nominal output current of 3.84 A. Fig. 15, and Table 6 demonstrates that the general control method divides the currents better than the other two methods. Thus, despite the initial prediction, the inverse loop control does not share input current properly.

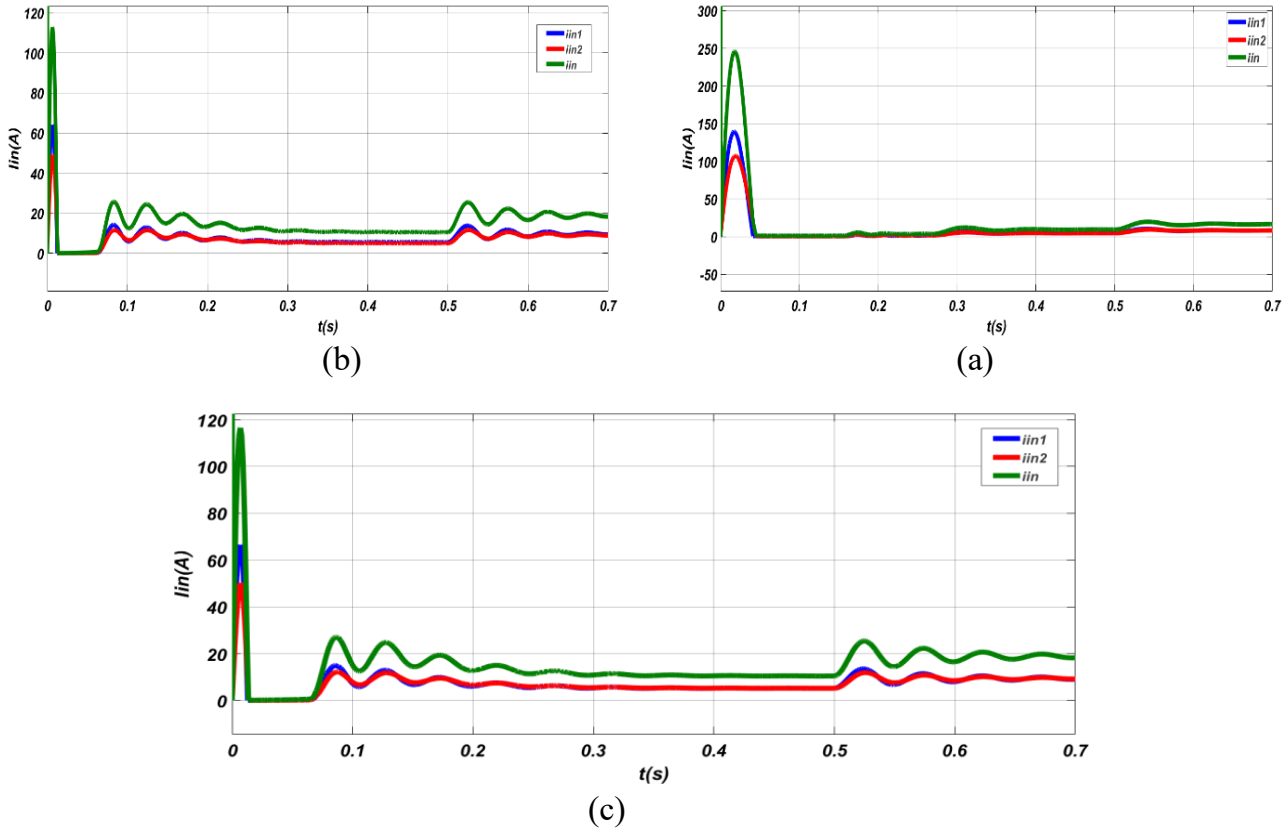

Fig. 15. Input currents (a) without control (b) with inverse-droop (c) with general control

Table 6. Comparison of input currents in three methods

Time(s)	I_{in1}-I_{in2}-I_{in}(A) (withoutcontrol)	I_{in1}-I_{in2}-I_{in}(A) (inversedroop)	I_{in1}-I_{in2}-I_{in}(A) (generalcontrol)
0-0.1	0.72-0.44-11.7	6-6.6-12.66	6.5-6.8-12.9
0.1-0.3	0.61-0.51-11.3	5.7-5.3-11	5.6-5.6-11.2
0.3-0.5	4.69-4.7-9.4	5.5-4.9-10.4	5.2-5.2-10.4
0.5-0.7	8.34-8.32-16.6	9.4-8.88-18.3	9.08-9.19-18.28

7- 4- Simulation of Circulation Current

Using the results in Fig. 16 and Table 7, it can be concluded, circulating current is reduced, in the systems with inverse-droop control and general control. In the general control method, the circulating current is more reduced, which proves effectively of the method from this point of view. For example, in time 0.5-0.7, circulating current in general control is 0.0000446 A, but in the inverse-droop control is 0.025. Additionally, with low circulating current, small losses are observed in the system with general control

7- 5- Comparison of Circulating Current

The results of circulating current simulation in this study are compared with the results of Ravi Kumar Gupta [7]. In [7], using the controller, the output current of both converters is almost the same. The RMS of the circulating current changed from 0.5545A to 0.1125A. According to Table 7 of this paper, the circulating current between two parallel common grounded z-source DC-DC converters in the inverse-droop method is 0.0188 A, and in the general control method is 0.00000238 A.

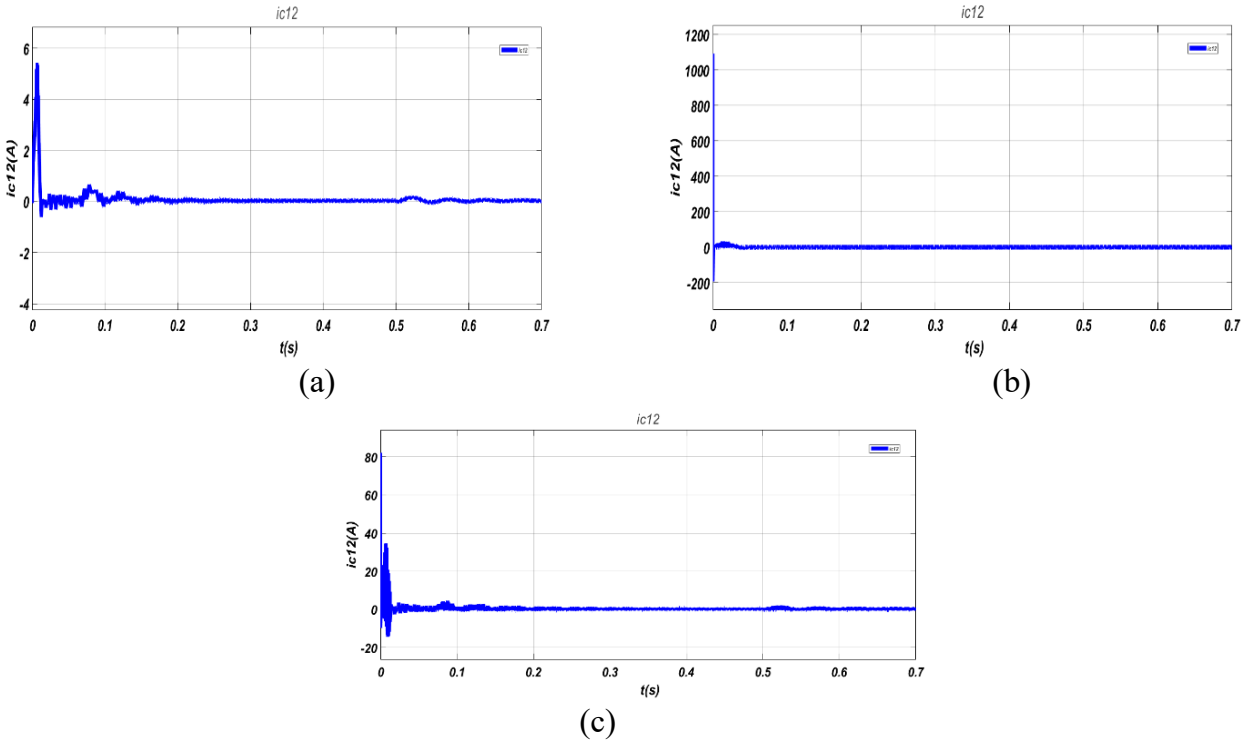

Fig. 16. Circulating current (a) without control (b) with inverse-droop control (c) with general control

Table 7. Comparison of circulating current in three methods

Time(s)	I_{c12} (A) (without control)	I_{c12} (A) (inverse-droop)	I_{c12}(A) (general-control)
0-0.1	0.0435	0.0095	0.000122
0.1-0.3	0.045	0.0035	0.000021
0.3-0.5	0.045	0.0188	0.00000238
0.5-0.7	0.89	0.16	0.0000446

In [24], an improved dynamic consensus-based distributed secondary control is proposed for a DC microgrid with converters of different rating connected in parallel operation. Load current is shared among converters according to their respective ratings. Compensated droop control is designed to minimize the circulating current through average circulating current control and can achieve the desired current sharing ratio.

Figs. 17 and 19 depict simulation for the system circulating currents without circulating current control and circulating current reduced with circulating current control of paper [24]. Note that in Fig.17, circulating current of converter 1, ic1, changes from 1A (before load change) to 1.8A (after load change), and converter 2, ic2, changes from −1A (before load change) to −1.8A. We can see in Fig. 19 that circulating current in converter 1, ic1, changes from 0.3A (before load change) to 0.49A (after load change) and converter 2, ic2, changes from −0.3A (before load change) to −0.49A. Figs. 18, 20 and 21 indicate simulation for the system circulating currents without control and droop control and general control under no-load in this paper. In Fig. 18, the circulating current is 0.0388A. We can see in Fig. 20 that the circulating current is 0.0326A. Note that in Fig. 21, circulating current is 0.008A.

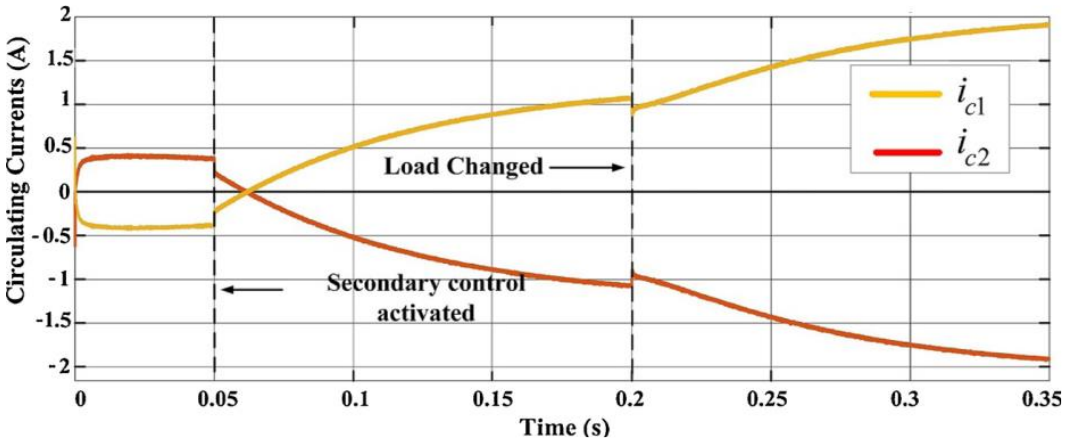

Fig. 17. Simulation for the system circulating currents without circulating current control [24]

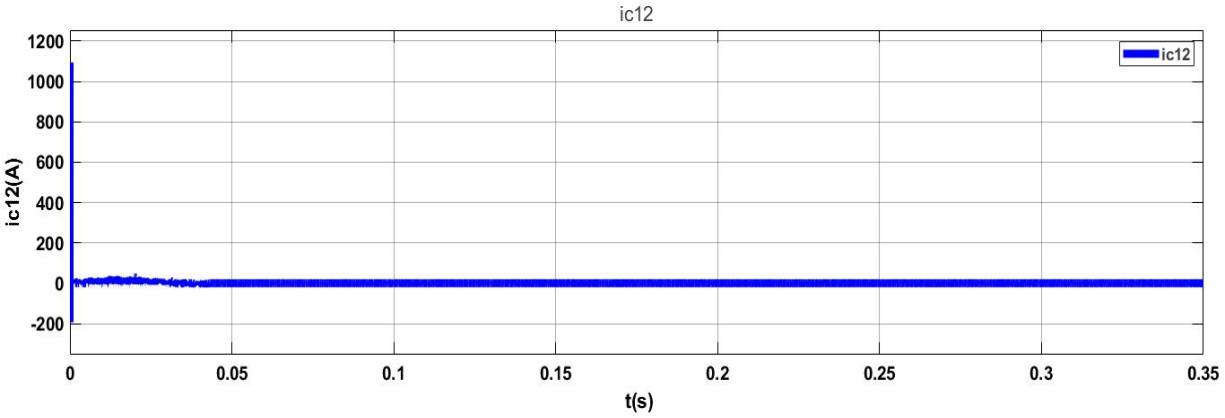

Fig. 18. Simulation circulating current under no-load

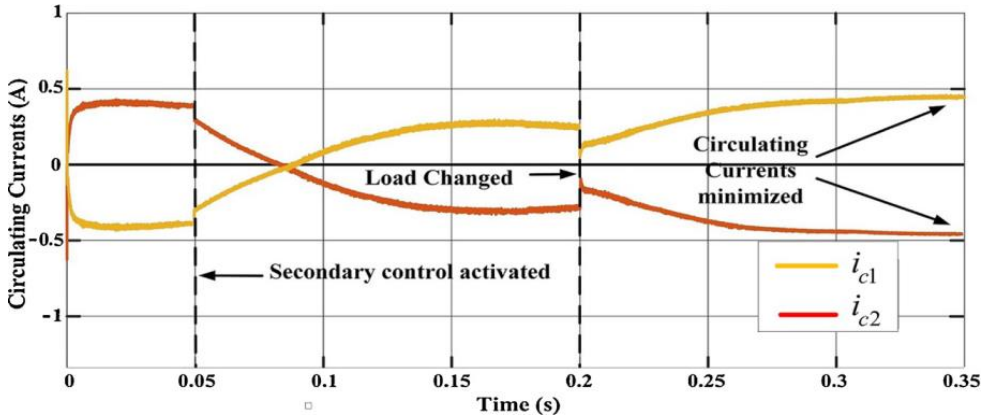

Fig. 19. Circulating current reduced with circulating current control [24]

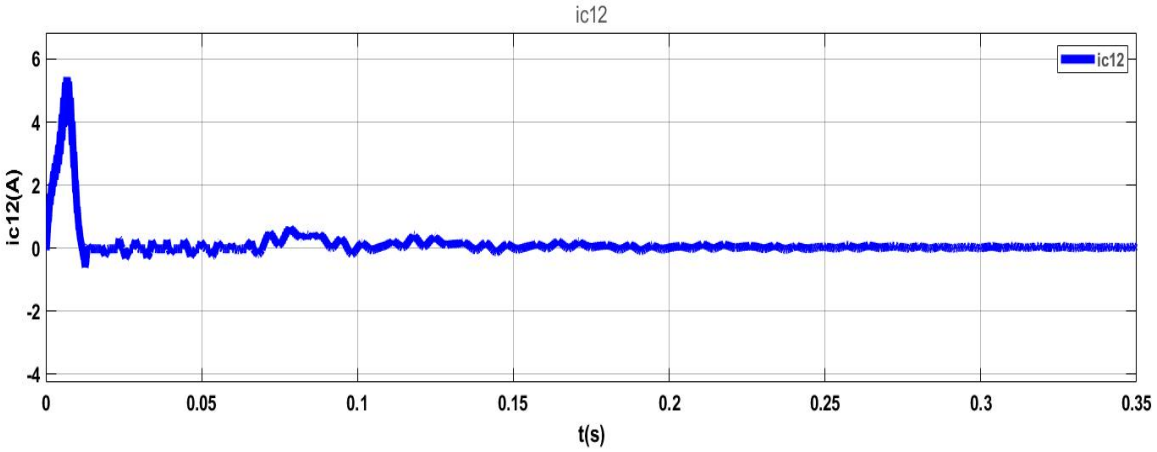

Fig. 20. Simulation circulating current for the proposed droop control under no-load

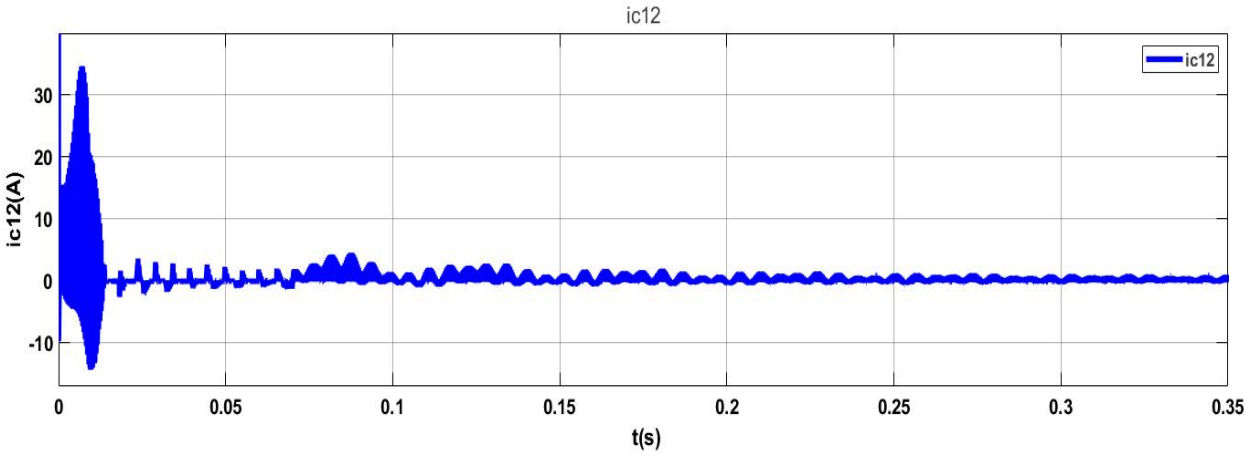

Fig. 21. Simulation circulating current for the proposed general control under no-load

8- Conclusion

One of the important goals in IPOP connection converters is power-sharing and reduction of circulating current among converters. For this purpose, we need control methods so that the input current and the output current are evenly divided between the converters. One of the most popular decentralized methods is the droop control method. Conventional droop control method has its disadvantages, such as poor voltage regulation, which the proposed inverse droop control method has eliminated, which is one of the most efficient centralized methods is the general control method. This paper proposes inverse-droop control and general control strategies for an IPOP connection between DC-DC converters. Decentralized inverse-droop control does not require communication among converters, which will increase capability, reduce cost, and complicate the system. The general control can be implemented for all four architectures: IPOP, IPOS, ISOS, ISOP without changing the structure, but the inverse-droop control is applicable only for two IPOP, ISOP architectures. The simulation results illustrate that the general control strategy has more excellent power-sharing (OCS and ICS) and dynamic characteristics than the inverse-droop control, even with parameters mismatch between the two converters. In the general control method, by dividing the Output Current (OCS), the input currents will be divided automatically. There is no need for separate control to divide the Input Current (ICS) and vice versa. The simulation results display the general control causes perfect current sharing and improves efficiency due to reduced circulating current.

Acknowledgment: Authors would like to acknowledge the financial support of Kermanshah University of Technology for this research under grant number S/P/T/T/21

References

[1] E. Rokrok, F. Shavakhi Zavareh, J. Soltani, M. Shakarami, "A Robust Control Strategy for Distributed Generations in Islanded Microgrids", in AUT Journal of Electrical Engineering, 52(1) (2020),107-120. DOI: 10.22060/eej.2019.14901.5246.

[2] S. Augustine, M. K. Mishra and N. Lakshminarasamma, "Adaptive Droop Control Strategy for Load Sharing and Circulating Current Minimization in Low-Voltage Standalone DC Microgrid," in IEEE Transactions on Sustainable Energy, 6 (2015 (132-141. doi: 10.1109/TSTE.2014.2360628.

[3] M. Rahideh, A. Halvaei Niasar, A. Ketabi, I. zamani, Linear Quadratic Integral optimal control of photovoltaic systems, AUT Journal of Electrical Engineering, 52(2) (2020) 231-242. DOI: 10.22060/eej.2020.14970.5249.

[4] E. Jafari, Determining the Optimal Strategy of Multi Virtual Power Plants using GA-GT, AUT Journal of Electrical Engineering, 52(2) (2020) 243-254. DOI: 10.22060/eej.2020.17607.5322.

[5] G. Xu, D. Sha and X. Liao, "Decentralized Inverse-Droop Control for Input-Series–Output-Parallel DC–DC Converters," in IEEE Transactions on Power Electronics, 30 (2015) 4621-4625. doi: 10.1109/TPEL.2015.2396898.

[6] J. Shi, L. Zhou and X. He, "Common-Duty-Ratio Control of Input-Parallel Output-Parallel (IPOP) Connected DC–DC Converter Modules with Automatic Sharing of Currents," in IEEE Transactions on Power Electronics, 27 (2012) 3277-3291. doi: 10.1109/TPEL.2011.2180541.

[7] Ravi Kumar Gupta, Vishnu Mohan Mishra, N.K. Singh, "Elimination of circulating current in parallel operation of single-phase inverter using droop controller", Engineering Science and Technology, an International Journal, (2021). https://doi.org/10.1016/j.jestch.2021.06.005.

[8] S. Augustine, N. Lakshminarasamma and M. K. Mishra, "Control of photovoltaic-based low-voltage dc microgrid system for power sharing with modified droop algorithm," in IET Power Electronics, 9 (2016) 1132-1143. doi: 10.1049/iet-pel.2015.0325.

[9] S. Anand, B.G. Fernandes, J. Guerrero, Distributed control to ensure proportional load sharing and improve voltage regulation in low-voltage dc microgrids, IEEE Trans. Power Electron. 28 (4) (2013) 1900 1913, https://doi.org/10.1109/TPEL.2012.2215055.

[10] J. Beerten, R. Belmans, Analysis of power sharing and voltage deviations in droop-controlled dc grids, IEEE Trans. Power Syst. 28 (4) (2013) 4588–4597, https://doi.org/10.1109/TPWRS.2013.2272494.

[11] D. Sha, Z. Guo, T. Luo and X. Liao, "A General Control Strategy for Input-Series–Output-Series Modular DC–DC Converters," in IEEE Transactions on Power Electronics, 29 (2014) 3766-3775. doi: 10.1109/TPEL.2013.2278546.

[12] X. Ruan, W. Chen, L. Cheng, C. K. Tse, H. Yan and T. Zhang, "Control Strategy for Input-Series–Output-Parallel Converters," in IEEE Transactions on Industrial Electronics, 56 (2009) 1174-1185. doi: 10.1109/TIE.2008.2007980.

[13] M. Abrehdari and M. Sarvi, "Comprehensive sharing control strategy for Input-Series Output-Parallel connected modular DC–DC converters," in IET Power Electronics, 12 (2019) 3105-3117. doi: 10.1049/iet-pel.2019.0054.

[14] D. Liu, F. Deng, Z. Gong and Z. Chen, " Input-Parallel Output-Parallel Three-Level DC/DC Converters with Interleaving Control Strategy for Minimizing and Balancing Capacitor Ripple Currents," in IEEE Journal of Emerging and Selected Topics in Power Electronics, 5 (2017) 1122-1132. doi: 10.1109/JESTPE.2017.2649221.

[15] W. Chen, G. Wang, X. Ruan, W. Jiang and W. Gu, "Wireless Input-Voltage-Sharing Control Strategy for Input-Series Output-Parallel (ISOP) System Based on Positive Output-Voltage Gradient Method," in IEEE Transactions on Industrial Electronics, 61 (2014) 6022-6030. doi: 10.1109/TIE.2014.2308147.

[16] Chin-Hsing Cheng, Po-Jen Cheng, Ming-Jia Xie, "Current sharing of paralleled DC–DC converters using GA-based PID controllers, "in Expert Systems with Applications, 37 (2010) 733-740.

[17] W. Chen and G. Wang, "Decentralized Voltage-Sharing Control Strategy for Fully Modular Input-Series–Output-Series System with Improved Voltage Regulation," in IEEE Transactions on Industrial Electronics, 62 (2015) 2777-2787. doi: 10.1109/TIE.2014.2365433.

[18] S. Rostami, V. Abbasi and F. Blaabjerg, "Implementation of a common grounded Z-source DC–DC converter with improved operation factors," in IET Power Electronics, 12 (2019) 2245-2255. doi: 10.1049/iet-pel.2018.6044.

[19] M. Rezaie and V. Abbasi, "Effective combination of quadratic boost converter with voltage multiplier cell to increase voltage gain," in IET Power Electronics, 13 (2020) 2322-2333. doi: 10.1049/iet-pel.2019.1070.

[20] J Barnabas Paul Glady, K Manjunath, "Analysis-intelligent design and simulation of improved state–space modelling for control of Luo converter," in Computers & Electrical Engineering, 75 (2019) 230-244.

[21] R. R. Ahrabi, H. Ardi, M. Elmi and A. Ajami, "A Novel Step-Up Multiinput DC–DC Converter for Hybrid Electric Vehicles Application," in IEEE Transactions on Power Electronics, 32 (2017) 3549-3561. doi: 10.1109/TPEL.2016.2585044.

[22] Nanfang Yang, Damien Paire, Fei Gao, Abdellatif Miraoui, Weiguo Liu, "Compensation of droop control

using common load condition in DC microgrids to improve voltage regulation and load sharing", in International Journal of Electrical Power & Energy Systems, 64 (2015) 752-760.

[23] L. Shu, W. Chen and X. Jiang, "Decentralized Control for Fully Modular Input-Series Output-Parallel (ISOP) Inverter System Based on the Active Power Inverse-Droop Method," in IEEE Transactions on Power Electronics, 33 (2018) 7521-7530. doi: 10.1109/TPEL.2017.2773559.

[24] Arshad Nawaz, Jing Wu, Chengnian Long, "Mitigation of circulating currents for proportional current sharing and voltage stability of isolated DC microgrid", in Electric Power Systems Research, 180 (2020) 106-123.

HOW TO CITE THIS ARTICLE

N. Amoozadeh, V. Abbasi, Control Strategy for Power Sharing in Input-Parallel and Output-Parallel Connected DC-DC Converters, AUT J Electr Eng, 55(1) (2023) 61-80.

DOI: 10.22060/eej.2022.21587.5484